Honam Mathematical J. **41** (2019), No. 2, pp. 403–420
https://doi.org/10.5831/HMJ.2019.41.2.403

APPROXIMATED SEPARATION FORMULA FOR THE HELMHOLTZ EQUATION

Ju-Hyun Lee[a], Nayoung Jeong[a], and Sungkwon Kang[b]

Abstract. The Helmholtz equation represents acoustic or electromagnetic scattering phenomena. The Method of Lines are known to have many advantages in simulation of forward and inverse scattering problems due to the usage of angle rays and Bessel functions. However, the method does not account for the jump phenomena on obstacle boundary and the approximation includes many high order Bessel functions. The high order Bessel functions have extreme blow-up or die-out features in resonance region obstacle boundary. Therefore, in particular, when we consider shape reconstruction problems, the method is suffered from severe instabilities due to the logical confliction and the severe singularities of high order Bessel functions. In this paper, two approximation formulas for the Helmholtz equation are introduced. The formulas are new and powerful. The derivation is based on Method of Lines, Huygen's principle, boundary jump relations, Addition Formula, and the orthogonality of the trigonometric functions. The formulas reduce the approximation dimension significantly so that only lower order Bessel functions are required. They overcome the severe instability near the obstacle boundary and reduce the computational time significantly. The convergence is exponential. The formulas adopt the scattering jump phenomena on the boundary, and separate the boundary information from the measured scattered fields. Thus, the sensitivities of the scattered fields caused by the boundary changes can be analyzed easily. Several numerical experiments are performed. The results show the superiority of the proposed formulas in accuracy, efficiency, and stability.

Received November 11, 2018. Accepted December 14, 2018.
2010 Mathematics Subject Classification. 65N40, 78A45, 35J05, 45G05.
Key words and phrases. Helmholtz equation, scattering, Method of Lines, Bessel functions, Addition Formula.
[a]First author
[b]Corresponding author

1. Introduction

The Helmholtz equation represents the scattering phenomena for acoustic or electromagnetic waves, and it has been investigated for many years. For examples, see [1, 2, 3, 4, 5, 7, 8, 10, 14, 16], and the references therein. Among many applications, the shape reconstructions have been known as highly nonlinear and severely ill-posed. In 2014, Lee and Kang[12, 13] introduced a unified complex nonlinear parameter estimation (CNPE) framework and a robust optimization algorithm for handling highly nonlinear and severe ill-posed problems. The CNPE framework and the corresponding robust algorithm solved successfully typical obstacle reconstruction problems. Those problems had been known as open problems in Inverse Scattering community for many decades[3]. The approximation for the obstacle shape was based on the global/spectral basis functions in [12] and the local/finite element basis functions in [13]. If we could estimate the obstacle boundary directly on the observation angles, it would be a powerful estimation scheme. This is a motivation of this paper.

The Method of Lines (MoL) were introduced in scattering problems by Ma et al.[15] and Hooshyar[6]. There are many advantages of MoL. We may list some of them as following[6, 15].

(i) It represents the solution on each observation angle, i.e., the scattering waves on each observation angle can be expressed separately.
(ii) On each observation angle, the solution can be expressed by a combination of the Bessel functions.
(iii) The computation of scattered fields is efficient.

However, the critical weak points of MoL are following.

(iv) It does not account for the jump phenomena on the boundary.
(v) It is consisted of all Hankel basis functions, i.e., all high order Bessel functions are required. The estimation of scattered fields near obstacle boundary is extremely unstable. For example, for the space dimension $N = 128$, MoL needs the Bessel functions or order approximately up to 40 (see Section 2). Since for the Bessel functions J and Y[11], $J_{40}(1) \approx 10^{-60}$ and $Y_{40}(1) \approx -10^{57}$ so that the forward and the inverse estimation processes by adjusting the coefficients of J_{40} and Y_{40} become extremely unstable.

The advantages (i)-(iii) of MoL mentioned above are strong points in conjunction with shape reconstruction aspects. On the other hand, the weak points (iv)-(v) above are critical issues. We need to overcome the weak points in order for considering the forward and inverse scattering problems. Specifically, the weak point (iv) is a logical confliction, i.e., the Helmholtz equation is valid only outside region of the obstacle. Thus, the differential equation can not be extended to the obstacle boundary. Therefore, we need to employ the boundary jump relation, and to reduce the number of approximation basis functions significantly.

The purpose of this paper is to derive a discrete scattering wave system having the strong points (i)-(iii) overcoming the weak points (iv)-(v). The basic ideas are following. By adopting Huygen's principle for the Helmholtz equation together with the jump relation on the boundary, the weak point (iv) can be solved. We apply the Addition Formula[3] to the fundamental kernel function to obtain approximated scattered fields on each observation angle. Since this approximation converges exponentially, the approximation dimension can be reduced significantly. For example, $M = 9$ or 13 is enough to achieve the accuracy 10^{-10} for the scattering fields for the space approximation dimension $N = 128$ or 256. That is, the Bessel functions of order up to 13 can be used for the approximation instead of including all Bessel functions up to order 40 or 81 (see Section 4). By applying the orthogonality properties of the trigonometric functions, the boundary information can be factored out completely from the measured scattered fields. The approximation procedures introduced in this paper is the continuously extended limiting case for the finite dimensional approximation by MoL (see Lemma 2.6 in Section 2). The formulas derived in this paper are not by MoL. But, they preserve the strong points of MoL without the weak points of MoL. Moreover, by separating the boundary information from the scattered fields, the sensitivity of scattered fields affected by boundary changes may be easily analyzed. The approximation formulas are new and powerful. The numerical experiments based on the proposed formulas show superiority in accuracy, efficiency, and stability.

The governing equation, Helmholtz equation, and the Method of Lines (MoL) are explained in Section 2. Some of strong points, weak points, and new findings for MoL are described in this section. In Section 3, two new powerful approximated separation formulas for the Helmholtz equation are derived. Based on the formulas derived in Section 3, the numerical simulations are performed in Section 4. The simulation results

show the superiority of the proposed formulas in accuracy, efficiency, and stability. The conclusion is in Section 5.

2. Helmholtz Equation and Method of Lines (MoL)

We consider the two-dimensional Helmholtz equation representing the scattering phenomena for a perfect electric conductor(PEC) or a sound-soft obstacle such as a metal. For such obstacles, incoming waves do not penetrate inside the obstacle. The governing equations are described as follows[3].

Let Ω be a PEC surrounded by a simple closed star-like C^2-boundary Γ in $\mathbb{R}^2$ and let Δ be the Laplace operator. Let $k > 0$ be the wave number such that k^2 is not a Dirichlet eigenvalue for $-\Delta$ in the interior of Ω. Let the incident plane wave with incident angle d be

$$u^{inc}(x) = e^{ikx\cdot d}, \quad x \in \mathbb{R}^2, \tag{2.1}$$

$$d = (\cos\theta, \sin\theta). \tag{2.2}$$

The total field u^o is defined by

$$u^o(x) = u^{inc}(x) + u^s(x), \quad x \in \mathbb{R}^2\backslash\Omega, \tag{2.3}$$

where u^s is the scattered field induced by the incident wave u^{inc} with direction vector d. Then the Helmholtz equation becomes

$$\Delta u^o + k^2 u^o = 0 \quad \text{in} \quad \mathbb{R}^2\backslash\overline{\Omega}, \tag{2.4}$$

$$u^o|_\Gamma = 0 \quad \text{on} \quad \Gamma = \partial\Omega, \tag{2.5}$$

$$\lim_{r\to\infty} \sqrt{r}\left(\frac{\partial u^s}{\partial r} - iku^s\right) = 0 \tag{2.6}$$

uniformly in all directions, where $r = |x|$, $\overline{\Omega}$ is the closure of Ω, $\Gamma = \partial\Omega$ is the boundary. The condition (2.5) shows perfect electric conducting or sound-soft property of the obstacle. The condition (2.6) for the scattering fields is called the *Sommerfeld radiation condition* and it ensures the uniqueness of the solution to (2.1)-(2.6) and guarantees that the scattering wave is outgoing. It is known that there exists a unique solution $u^o \in C^2(\mathbb{R}^2\backslash\overline{\Omega})\bigcap C(\mathbb{R}^2\backslash\Omega)$.

Remark 2.1. *(i) The incoming incident plane wave (2.1) propagates perpendicularly to the obstacle axis. (ii) The boundary condition (2.5) for the total field shows that* $u^s(x) = -u^{inc}(x)$ *on the boundary* Γ *due to (2.3). Recall that the incident wave cannot penetrate the inside of the sound-soft obstacle. This means that equation (2.4) is valid only outside of the obstacle. (iii) Both the incident wave* u^{inc} *and the scattering wave* u^s *satisfy the Helmholtz equation (2.4).*

Remark 2.2. *(i) It has been well-known that, based on the measurements of the scattered fields, the problem of finding the obstacle shape is highly nonlinear and severely ill-posed. (ii) Many integral representations for equation (2.4) are available. Among them, the typical double- and single-layer potential representation contains the jump phenomena on the boundary. Therefore, a special numerical scheme for solving the jump equation is required. The Nyström method with Gauss quadrature rule has proven to be stable and accurate*[3].

We now describe the Method of Lines (MoL)[6, 9, 15] for the Helmholtz equation. The methodology, the strong points and the weak points of MoL are explained briefly. Since the ideas, concepts, strong points as well as weak points of MoL are important for the derivation of a new approximation formula for computing scattering fields, we describe briefly some of known results, corrected results, and new findings.

Recall that the scattering wave u^s satisfies equation (2.4). i.e.,

$$\Delta u^s(x) + k^2 u^s(x) = 0 \quad \text{in} \quad \mathbb{R}^2 \backslash \overline{\Omega}. \tag{2.7}$$

By polar coordinate system, equation (2.7) can be represented by

$$\left(\frac{\partial^2}{\partial r^2} + \frac{1}{r}\frac{\partial}{\partial r} + \frac{1}{r^2}\frac{\partial^2}{\partial \theta^2} + k^2 \right) F(r, \theta) = 0, \tag{2.8}$$

where $F(r, \theta)$ is the transformed scattered fields $u^s(x)$ in (2.7), $r = |x|$, θ is angle.

Let N be an approximation dimension. Let

$$\Delta\theta = \frac{2\pi}{N}, \quad \theta_j = j\Delta\theta, \quad 0 \le j \le N-1. \tag{2.9}$$

Let

$$F = [F_0, F_1, \cdots, F_{N-1}]^T, \tag{2.10}$$

$$F_j = F(r, \theta_j), \quad 0 \le j \le N-1, \tag{2.11}$$

$$D = \begin{bmatrix} 2 & -1 & 0 & \cdots & 0 & 0 & -1 \\ -1 & 2 & -1 & \cdots & 0 & 0 & 0 \\ 0 & -1 & 2 & \cdots & 0 & 0 & 0 \\ \vdots & \vdots & \vdots & \ddots & \vdots & \vdots & \vdots \\ 0 & 0 & 0 & \cdots & 2 & -1 & 0 \\ 0 & 0 & 0 & \cdots & -1 & 2 & -1 \\ -1 & 0 & 0 & \cdots & 0 & -1 & 2 \end{bmatrix}_{N \times N}, \tag{2.12}$$

where we denote A^T the transpose of a vector or a matrix A.
Then we have the following discretized system

$$\frac{d^2}{dr^2}F + \frac{1}{r}\frac{dF}{dr} + k^2 F - \frac{D}{(r\Delta\theta)^2}F = 0. \tag{2.13}$$

It is known[9, 15] that the matrix D can be factorized by the orthonormal transformation Q such that

$$\Lambda = Q^T D Q, \tag{2.14}$$

$$Q^T = Q^{-1}, \tag{2.15}$$

where the $N \times N$ diagonal matrix Λ with diagonal entries λ_j, is the j-th eigenvalue of D, and the j-th column Q_j of Q is consisted of the corresponding eigenvector with respect to the eigenvalue $\lambda_j, 0 \le j \le N-1$.

Remark 2.3. *The eigen pairs* $(\lambda_j, Q_j), 0 \le j \le N-1$, *for the matrix* D *can be obtained explicitly*[9, 15]. *More specifically,*

$$\lambda_j = 4\sin^2\frac{j\pi}{N}, \quad j = 0, 1, \cdots, N-1, \tag{2.16}$$

when N *is even, for each* j, $0 \le j \le N-1$,

$$Q_{jm} = \begin{cases} \frac{1}{\sqrt{N}}, & m = 0, \\ \sqrt{\frac{2}{N}}\cos\frac{2jm}{N}\pi, & m = 1, 2, \cdots, \frac{N}{2}-1, \\ \frac{1}{\sqrt{N}}\cos j\pi, & m = \frac{N}{2}, \\ -\sqrt{\frac{2}{N}}\sin\frac{2jm}{N}\pi, & m = \frac{N}{2}+1, \cdots, N-1, \end{cases} \tag{2.17}$$

when N is odd,

$$Q_{jm} = \begin{cases} \frac{1}{\sqrt{N}}, & m = 0, \\ \sqrt{\frac{2}{N}} \cos \frac{2jm}{N}\pi, & m = 1, 2, \cdots, \frac{N-1}{2}, \\ -\sqrt{\frac{2}{N}} \sin \frac{2jm}{N}\pi, & m = \frac{N+1}{2}, \cdots, N-1, \end{cases} \tag{2.18}$$

where Q_{jm} is an (j, m) element of $[Q]$. For more detailed derivation of the above eigen pairs, see [6, 9, 15].

Let

$$u = Q^T F. \tag{2.19}$$

The equation (2.13) becomes

$$\frac{d^2}{dr^2}u_j(r) + \frac{1}{r}\frac{d}{dr}u_j(r) + k^2 u_j(r) - \frac{\lambda_j}{(r\Delta\theta)^2}u_j(r) = 0, \quad 0 \le j \le N-1. \tag{2.20}$$

Remark 2.4. [3, 6, 9, 15] *The equation (2.20) is the Bessel equation with order*

$$\nu_j = \frac{\sqrt{\lambda_j}}{\Delta\theta}, \tag{2.21}$$

and the solution can be expressed as

$$u_j(r) = A_j H^{(1)}_{\nu_j}(kr), \tag{2.22}$$

where A_j is the coefficient, and $H^{(1)}_{\nu_j}$ is the Hankel function of the first kind order ν_j,

$$H^{(1)}_{\nu_j}(kr) = J_{\nu_j}(kr) + iY_{\nu_j}(kr), \tag{2.23}$$

$$J_{\nu_j}(kr) := \sum_{p=0}^{\infty} \frac{(-1)^p}{p!(\nu_j + p)!}\left(\frac{kr}{2}\right)^{\nu_j+2p}, \quad kr \in \mathbb{R}, \tag{2.24}$$

$$\begin{aligned} Y_{\nu_j}(kr) := {} & \frac{2}{\pi}\{\ln\frac{kr}{2} + C\}J_{\nu_j}(kr) - \frac{1}{\pi}\sum_{p=0}^{\nu_j-1}\frac{(\nu_j - 1 - p)!}{p!}\left(\frac{2}{kr}\right)^{\nu_j-2p} \\ & -\frac{1}{\pi}\sum_{p=0}^{\infty}\frac{(-1)^p}{p!(\nu_j+p)!}\left(\frac{kr}{2}\right)^{\nu_j+2p}\{\psi(p+\nu_j)+\psi(p)\}, \ \nu_j = 0, 1, 2, \ldots, \end{aligned} \tag{2.25}$$

where we denote $\psi(0) := 0, \psi(p) := \sum_{m=1}^{p}\frac{1}{m}, p = 1, 2, \cdots$ and $C := \lim_{p\to\infty}\{\sum_{m=1}^{p}\frac{1}{m} - \ln p\}$ is the Euler constant.

Remark 2.5. [9] *For the space approximation dimension $N = 128$ or 256, the order ν defined by (2.21) has range approximately $0 \le \nu \le 40.7$ for $N = 128$ and $0 \le \nu \le 81.5$ for $N = 256$. Some of the Bessel function values are following.*
$J_{40}(1) \approx 1.1079 \times 10^{-60}$ and $Y_{40}(1) \approx -7.1849 \times 10^{57}$, i.e., for a high order ν, $J_\nu(t)$ has almost negligible values and $Y_\nu(t)$ has extremely large values for small $t > 0$. Thus, for example, the estimation processes of an obstacle boundary become extremely unstable. It is necessary to reduce the number of J_{ν_j} and Y_{ν_j} as much as possible to consider forward as well as inverse scattering problems.

Lemma 2.6. *Let ν_j, $0 \le j \le N-1$, be the Bessel function order defined by (2.21). Then, for a fixed j, $\nu_j \to j$ as $N \to \infty$.*

Proof. From the following relation

$$\nu_j = \frac{\sqrt{\lambda_j}}{\Delta\theta} = \frac{\sqrt{4\sin^2\frac{j\pi}{N}}}{\frac{2\pi}{N}} = \left|\sin\frac{j\pi}{N}\right| \frac{N}{\pi},$$

we have

$$\lim_{N\to\infty} \nu_j = \lim_{N\to\infty} \left|\sin\frac{j\pi}{N}\right| \frac{N}{\pi} = \lim_{N\to\infty} \frac{\left|\sin\frac{j\pi}{N}\right|}{\left|\frac{j\pi}{N}\right|} \left|\frac{j\pi}{N}\right| \frac{N}{\pi} = j.$$

□

Remark 2.7. *(i) In MoL, the coefficients $A_j, 0 \le j \le N-1$, in equation (2.22) are obtained by considering the boundary condition (2.5), i.e.,*

$$F_j(r) = \sum_{l=0}^{N-1} Q_{j,l+1} A_l H_{\nu_l}^{(1)}(kr), \quad 0 \le j \le N-1. \tag{2.26}$$

This means that the differential equation (2.20) could be extended continuously to the obstacle boundary. However, for a PEC or a sound-soft obstacle, the differential equation is valid only outside of the obstacle. Therefore, it is necessary to consider the boundary jump relation as mentioned before.
(ii) The expression (2.26) has strong advantages in computation of scattered fields due to the use of semi analytic functions. Also, the scattering waves are computed separately on each individual observation angles. These two aspects are strong points of MoL.

3. Approximated separation formula

In this section, we derive two approximated separation formulas for the scattering waves governed by the Helmholtz equation (2.4). The derivation is based on the Huygen principle, the boundary jump relations, the Addition Formula, and the orthogonality of the trigonometric functions. In the formulas, the boundary information are separated completely from the measured scattered fields. Moreover, the scattering waves are expressed along the observation angles. Also, the formulas lead significant reduction of approximation dimension so that only low order Bessel functions can be used for computation of scattered fields. The formulas are new and powerful in terms of accuracy, efficiency, and stability. We can see the superiority of the proposed formulas in the next numerical section.

It is well-known that the scattered field $u^s(x)$ can be represented by the following integral formula using the Huygen principle[3].

$$u^s(x) = -\int_\Gamma \Phi(x,y)\frac{\partial u^o}{\partial \nu}(y)ds(y), \quad x \in \mathbb{R}^2\backslash\overline{\Omega}, \tag{3.1}$$

where

$$\Phi(x,y) = \frac{i}{4}H_0^{(1)}(k|x-y|), \tag{3.2}$$

$H_0^{(1)}$ is the Hankel function of the first kind order 0 defined by

$$H_0^{(1)} = J_0 + iY_0. \tag{3.3}$$

J_0 and Y_0 are the Bessel functions of order 0 defined by (2.23)-(2.25) with $\nu_j = 0$.

We now consider the following addition formula for the Hankel function $H_0^{(1)}$ of the first kind order 0.

Lemma 3.1. (Addition Formula [3]**)** *Let $x, y \in \mathbb{R}^2$ be two vectors with $|x| > |y|$ and let θ be the angle between x and y. Then*

$$H_0^{(1)}(k|x-y|) = H_0^{(1)}(k|x|)J_0(k|y|) + 2\sum_{m=1}^{\infty} H_m^{(1)}(k|x|)J_m(k|y|)\cos m\theta. \tag{3.4}$$

Remark 3.2. *(i) From (3.4), we may approximate* $H_0^{(1)}(k|x-y|)$ *with* $|x| > |y|$ *by*

$$H_0^{(1)}(k|x-y|) \approx H_0^{(1)}(k|x|)J_0(k|y|) + 2\sum_{m=1}^{M-1} H_m^{(1)}(k|x|)J_m(k|y|)\cos m\theta, \tag{3.5}$$

where M *is the approximation dimension for (3.4).*
(ii) In the Huygen principle (3.1), the kernel function $\Phi(x,y)$ *can be approximated by the formula (3.5). In this case, we take the vector* y *the boundary position vector and* x *the scattering field measuring position vector.*
(iii) In formula (3.5), the approximation dimension M *should be small compared with the space discretization dimension* N*. From our numerical experiments,* M *turns out to be significantly small compared with* N *for most cases. For example,* $M = 13$ *is enough for* $N = 128$ *or* $N = 256$ *to achieve the accuracy* 10^{-10} *(see Section 4).*

We now derive the approximated separation formulas for the scattered fields $u^s(x)$ in (3.1). They look complicated. However, the formulas are surprisingly powerful in terms of accuracy as well as computing efficiency.

Theorem 3.3. (Separation Formula 1) *Let* $(x_i, \theta_i), 0 \le i \le N-1$, *be the measuring position pair with position* x_i *at angle* θ_i *with* $|x_i| = r$ *for the scattered field* u^s *in (3.1). Let*

$$u^s(x_i,\theta_i) = \sum_{m=0}^{M-1} c_{im} H_m^{(1)}(k|x_i|), \quad 0 \le i \le N-1, \tag{3.6}$$

i.e.,

$$\begin{bmatrix} u^s(r,\theta_0) \\ u^s(r,\theta_1) \\ u^s(r,\theta_2) \\ \vdots \\ u^s(r,\theta_{N-1}) \end{bmatrix}$$

$$= \begin{bmatrix} c_{00} & c_{01} & c_{02} & \cdots & c_{0,M-1} \\ c_{10} & c_{11} & c_{12} & \cdots & c_{1,M-1} \\ c_{20} & c_{21} & c_{22} & \cdots & c_{2,M-1} \\ \vdots & \vdots & \vdots & \cdots & \vdots \\ c_{N-1,0} & c_{N-1,1} & c_{N-2,2} & \cdots & c_{N-1,M-1} \end{bmatrix} \begin{bmatrix} H_0^{(1)}(kr) \\ H_1^{(1)}(kr) \\ H_2^{(1)}(kr) \\ \vdots \\ H_{M-1}^{(1)}(kr) \end{bmatrix}.$$

Then, for $0 \le j \le N-1$, we obtain the coefficients c_{im} in terms of the boundary information.

$$c_{i0} = (-\Delta\theta)\left(\frac{\sqrt{-1}}{4}\right)(1)\sum_{j=0}^{N-1}\alpha_j J_0(kR_j), \tag{3.7}$$

$$c_{im} = (-\Delta\theta)\left(\frac{\sqrt{-1}}{4}\right)(2)\sum_{j=0}^{N-1}\cos(|i-j|(m\Delta\theta))\alpha_j J_m(kR_j), \tag{3.8}$$

where $1 \le m \le M-1$,

$$\alpha_j = \left(\frac{\partial u^o}{\partial \nu_j}\right)\sqrt{(R_j{}')^2 + (R_j)^2}, \tag{3.9}$$

u^o is the total field,

$$\frac{\partial u^o}{\partial \nu_j} = \frac{\partial u^o(y)}{\partial \nu_j(y)} = \frac{\partial u^o(y_j,\theta_j)}{\partial \nu_j(y_j,\theta_j)} \tag{3.10}$$

is the normal derivative of the total field u^o at $y \in \Gamma$ with angle θ_j.

$$R_j = |y_j|,\ y_j = y(\theta_j) \in \Gamma,\ 0 \le j \le N-1, \tag{3.11}$$

where $R_j{}' = \frac{\partial R_j}{\partial \theta}(\theta_j)$ is the angle derivative of R_j and $\Delta\theta = \frac{2\pi}{N}$.

Proof. Let N be the space approximation dimension for $[0, 2\pi]$, and let $\Delta\theta$, $\theta_j = (j)\Delta\theta$, $0 \le j \le N-1$, be the angle increments defined by (2.9). Since the obstacle is star-like shape, we may express the boundary Γ as

$$y(\theta) = R(\theta)\begin{pmatrix}\cos\theta \\ \sin\theta\end{pmatrix}, \quad 0 \le \theta \le 2\pi. \tag{3.12}$$

Let the angle division θ_j and the corresponding boundary position vector y_j with radius $R_j = |y_j|, 0 \le j \le N-1$. Then the outward normal vector ν_j at $y_j \in \Gamma$ becomes

$$\nu_j = \nu(y_j) = \frac{(y_{j2}{}', -y_{j1}{}')}{|y_j{}'|} \tag{3.13}$$

where $y_j = (y_{j1}, y_{j2}) \in \Gamma$, $'$ denotes the angle derivative. Since

$$y_j{}' = \begin{pmatrix} y_{j1}{}' \\ y_{j2}{}' \end{pmatrix} = \begin{pmatrix} R_j{}' \cos\theta_j - R_j \sin\theta_j \\ R_j{}' \sin\theta_j + R_j \cos\theta_j \end{pmatrix},$$
$$\nu_j = \frac{1}{\sqrt{(R_j{}')^2 + (R_j)^2}} \begin{pmatrix} R_j{}' \cos\theta_j - R_j \sin\theta_j \\ R_j{}' \sin\theta_j + R_j \cos\theta_j \end{pmatrix}. \tag{3.14}$$

On the other hand,

$$\begin{aligned} ds(y) &= \sqrt{\left(\frac{dy_1(\theta)}{d\theta}\right)^2 + \left(\frac{dy_2(\theta)}{d\theta}\right)^2} d\theta \\ &= |y'| d\theta = \sqrt{(R_j{}')^2 + (R_j)^2} d\theta. \end{aligned} \tag{3.15}$$

We now plug the approximation addition formula (3.5) into the kernel $\Phi(x, y)$ in (3.2). After some manipulation, we have the separation formula described in the theorem. Here, the normal derivative $\frac{\partial u^o}{\partial \nu}(y)$ of the total field u^o is obtained from the boundary jump relation[3]

$$\begin{aligned} &\frac{\partial u^o}{\partial \nu}(x) + 2\int_\Gamma \{\frac{\partial \Phi(x,y)}{\partial \nu(x)} - i\eta\Phi(x,y)\} \frac{\partial u^o}{\partial \nu}(y) ds(y) \\ &\qquad = 2\frac{\partial u^{inc}}{\partial \nu}(x) - 2i\eta u^{inc}(x), \quad x \in \partial D, \end{aligned} \tag{3.16}$$

where η is a coupling parameter. This completes the proof. □

Remark 3.4. *(i) The coefficient matrix $[c_{im}]$ contains only the obstacle boundary information. (ii) It is well-known that the jump boundary equation (3.16) for $\frac{\partial u^o}{\partial \nu}(y)$ can be efficiently solved by the Nyström method with the Gauss Quadrature*[3].

After careful observation on the orthogonality of the discrete trigonometric functions appeared in the matrix $[c_{im}]$ in Theorem 3.3, we have the following second separation formula.

Theorem 3.5. (Separation Formula 2) *Let*

$$[P(:,1)]^T = \left[\sqrt{\frac{1}{N}}, \sqrt{\frac{1}{N}}, \sqrt{\frac{1}{N}}, \cdots, \sqrt{\frac{1}{N}} \right], \tag{3.17}$$

$$\begin{aligned} [P(:,m+1)]^T = [\quad &\sqrt{\tfrac{2}{N}}, \sqrt{\tfrac{2}{N}}\cos(1 \cdot m\Delta\theta), \sqrt{\tfrac{2}{N}}\cos(2 \cdot m\Delta\theta), \\ &\cdots, \sqrt{\tfrac{2}{N}}\cos((N-1) \cdot m\Delta\theta)], \quad 1 \le m \le M-1. \end{aligned} \tag{3.18}$$

Then we have

$$\begin{aligned}&\alpha_0 J_0(kR_0)+\alpha_1 J_0(kR_1)+\alpha_2 J_0(kR_2)+\cdots+\alpha_{N-1}J_0(kR_{N-1})\\&=\left(\frac{2\sqrt{N}}{\pi}\sqrt{-1}[P(:,1)]^T[u^s(x_i)]_{0\le i\le N-1}\right)/H_0^{(1)}(kr),\end{aligned}\tag{3.19}$$

$$\begin{aligned}&1\cdot\alpha_0 J_m(kR_0)+\cos(1\cdot m\Delta\theta)(\alpha_1 J_m(kR_1))+\cos(2\cdot m\Delta\theta)(\alpha_2 J_m(kR_2))\\&+\cdots+\cos((N-1)\cdot m\Delta\theta)(\alpha_{N-1}J_m(kR_{N-1}))\\&=\left(\frac{2\sqrt{N}}{\pi}\sqrt{-1}[P(:,m+1)]^T[u^s(x_i)]_{0\le i\le N-1}\right)/H_m^{(1)}(kr),\end{aligned}\tag{3.20}$$

where $1\le m\le M-1$, $r=|x_i|,\quad 0\le i\le N-1$,

$$\alpha_j=\left(\frac{\partial u^o}{\partial\nu_j}\right)\sqrt{(R_j{}')^2+(R_j)^2},$$

u^o *is the total field,* $R_j=|y(\theta_j)|,\quad y(\theta_j)\in\Gamma$, $R_j{}'=\left(\frac{d}{d\theta}R(\theta)\right)|_{\theta=\theta_j}$, $\nu_j=\nu(y(\theta_j))=$ *the outward normal unit vector at* $y(\theta_j)\in\Gamma$.

Proof. The formula in this theorem is obtained from the discretized orthogonality property of the trigonometric function. From the first separation formula in Theorem 3.3, by some manipulation, we have the following relation.

$$\left(\sqrt{\frac{1}{N}}\right)\left(\sum_{i=0}^{N-1}c_{i0}\right)H_0^{(1)}(kr)=[P(:,1)]^T[u^s(x_i)]_{0\le i\le N-1},\tag{3.21}$$

$$\left(\sqrt{\frac{1}{N}}\right)\sum_{i=0}^{N-1}c_{im}=0,\quad 1\le m\le M-1\tag{3.22}$$

For each m, $1\le m\le M-1$, $0\le l\le M-1$,

$$[P(:,m+1)]^T[c_{il}]H_m^{(1)}(kr)=\begin{cases}[P(:,m+1)]^T[u^s(x_i)]_{0\le i\le N-1}, & l=m,\\ 0, & l\ne m,\end{cases}\tag{3.23}$$

The above relations (3.22) and (3.23) come from the orthogonality of the cosine functions. This completes the proof. □

Remark 3.6. *(i) The Hankel functions* $H_m^{(1)}(kr)$ *in Theorem 3.5 are not zero for all* m, $0\le m\le M-1$. *(ii) In (3.19) and (3.20), the boundary information such as* $J_m(kR_j),\alpha_j$ *and the information on the*

measuring positions x_i, i.e., the distance r, are completely separated by left- and right-hand sides.

4. Implementation and numerical results

In this section, the numerical experiments are performed to show the accuracy as well as the efficiency of the proposed separation formulas derived in Section 3. Many examples including a kite, a moved circle, a peanut, a round rectangle, and a non-symmetric obstacle commonly adopted in the scattering literature were used for our simulations. The numerical results were almost similar. Among the examples, the computation results for a kite, a peanut, and a non-symmetric obstacle are shown. These examples have both convex and concave shapes so that it is well-known that the approximation or recovery estimation processes are slow or difficult.

The numerical experiments were performed under MATLAB environment using a conventional personal computer. The algorithms were not optimized. However, based on the formulas derived in Section 3, the computational results show superiority in accuracy, efficiency, and stability with small approximation dimension M. For most examples, $M = 9 \sim 13$ were enough to achieve the discrete L^2 accuracy 10^{-10} for the space dimension $N = 128$ or $N = 256$. For the simulations, the wave number $k = 1$ is used.

Example 4.1. (Kite) *The kite can be parameterized as*

$$\Gamma : x(t) = \begin{pmatrix} x_1(t) \\ x_2(t) \end{pmatrix}, \begin{array}{ll} x_1(t) & = \cos t + 0.65(\cos 2t \ - 1) \\ x_2(t) & = 1.5 \sin t, \quad 0 \le t \le 2\pi. \end{array} \tag{4.1}$$

The expression of this example is not of a star-shaped form. By an appropriate variable changes, the expression can be transformed into a star-shaped form.

Example 4.2. (Peanut)

$$x_1(t) = R(t)\cos t, \ x_2(t) = R(t)\sin t, \ R(t) = 0.5\sqrt{3\cos^2 t + 1}. \tag{4.2}$$

Example 4.3. (Non-symmetric obstacle)

$$x_1(t) = R(t)\cos t, \ x_2(t) = R(t)\sin t, \ R(t) = \frac{1 + 0.9\cos t + 0.1\sin 2t}{1 + 0.75\cos t}. \tag{4.3}$$

Figures 1(a)-(c) show the obstacle shapes. It is easy to see that the obstacles have both convex and concave profiles.

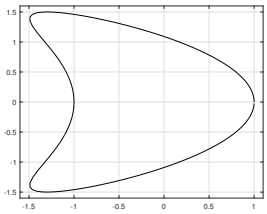

Fig. 1(a). Kite

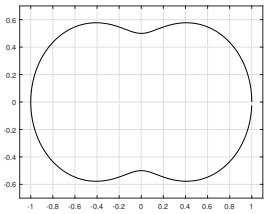

Fig. 1(b). Peanut

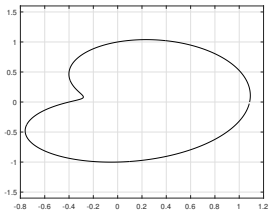

Fig. 1(c). Non-symmetric

Table 1 shows the approximation L^2-errors for the examples. The incident angle $\theta = 0$, observation distance $r = 20$ were chosen. It was observed that the approximation dimensions $M = 9 \sim 13$ were enough to achieve the accuracy 10^{-10} for the space dimension $N = 128$ or $N = 256$ as mentioned in the beginning of this section. In Table 1, the errors were estimated compared with the solution for $N = 128$. Surprisingly, the convergence were exponential with decay rates $2.3 \sim 3.3$.

TABLE 1. L^2-Errors ($\theta = 0,\ \rho = 20,\ N = 128$)

M	Kite	Peanut	Non-symmetric
8	5.8117×10^{-5}	6.5625×10^{-9}	1.2572×10^{-8}
9	4.9646×10^{-6}	6.6982×10^{-11}	3.4692×10^{-10}
10	1.3488×10^{-7}	4.8148×10^{-12}	1.4307×10^{-11}
12	4.6584×10^{-9}	3.7840×10^{-15}	1.2218×10^{-14}
13	2.8728×10^{-10}	2.6077×10^{-15}	3.0377×10^{-15}
14	5.7970×10^{-12}	2.6076×10^{-15}	3.0227×10^{-15}

Figures 2-4 show the comparison of the scattered fields for $N = 128$ and the approximated ones by $M = 13$. In the figures, (a) shows the magnitude and (b) shows the phase angle. The solid lines are the true scattered fields for $N = 128$ and the dotted lines are the approximated u^s by $M = 13$. It is easy to notice that the two lines are not distinguishable due to the small errors as shown in Table 1.

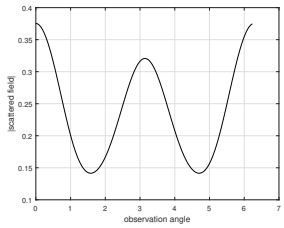

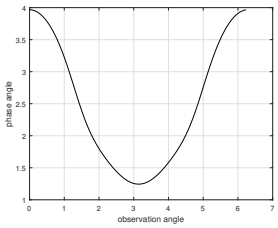

Fig. 2(a). $|u^s|$ Fig. 2(b). Angle(u^s)
Kite

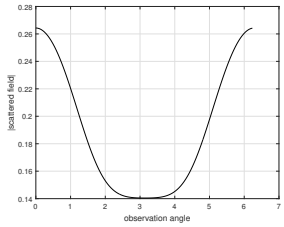

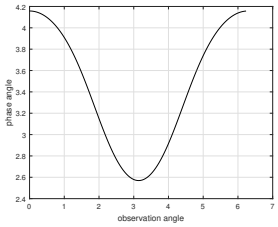

Fig. 3(a). $|u^s|$ Fig. 3(b). Angle(u^s)
Peanut

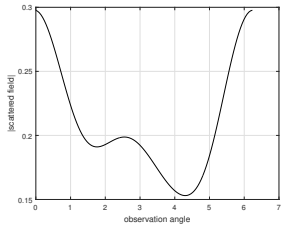

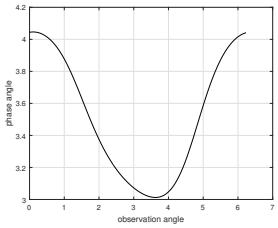

Fig. 4(a). $|u^s|$ Fig. 4(b). Angle(u^s)
Non-symmetric

5. Conclusion

Two approximation formulas for the two dimensional Helmholtz equation representing a sound-soft obstacle or a perfect electric conductor are derived. The formulas are new and powerful. They are derived based on the Huygen principle, the boundary jump relation, the Addition Formula, and the orthogonality of the trigonometric functions. The proposed formulas have the advantages of the Method of Lines (MoL), and overcome the disadvantages of MoL. Moreover, in the formulas, the boundary information from the measured scattered fields are completely separated so that the relations between obstacle shapes and corresponding scattered fields can be analysed easily. The two proposed formulas are applied to the typical examples commonly used in the scattering literature. The simulation results show the superiority in accuracy, efficiency, and stability.

Acknowledgments

The research by S. Kang was supported by Basic Science Research Program through the National Research Foundation of Korea (NRF) funded by the Ministry of Education, Science and Technology (Grant NRF 2010-0010906), and also supported by Chosun University.

References

[1] H. Ammari, *An Introduction to Mathematics of Emerging Biomedical Imaging (Mathematiques et Application)*, Springer, 2008.

[2] M. Belonosov, M. Dmitriev, V. Kostin, D. Neklyudov, V. Tcheverda, *An iterative solver for the 3D Helmholtz equation*, J. Computational Physics **345** (2017), 330-344.

[3] D. Colton and R. Kress, *Inverse Acoustic and Electromagnetic Scattering Theory (3rd Ed)*, Springer, Berlin, 2013.

[4] U. Guo, F. Ma, and D. Zhang, *An optimization method for acoustic inverse obstacle scattering problems with multiple incident waves*, Inverse Problems in Science and Engineering **19** (2011), 461-484.

[5] B. Guzina, F. Cakoni, and C. Bellis, *On multi-frequency obstacle reconstruction via linear sampling method*, Inverse Problems **26** (2010) 125005(29pp).

[6] M. Hooshyar, *An inverse problem of electromagnetic scattering and the Method of Lines*, Microwave and Optical Technology Letters, **29(6)** (2001), 420-426.

[7] O. Ivanyshyn, *Shape reconstruction of acoustic obstacles from the modulus of the far field pattern*, Inverse Problems and Imaging Vol 1 No 4(2007), 609-622.

[8] O. Ivanyshyn and T. Johansson, *Nonlinear integral equation methods for the reconstruction of an acoustically sound-soft obstacle*, Journal of Integral equations and applications Vol 19 No 3 (2007), 289-308.
[9] N. Jeong, *Inverse Scattering Problem Based on the Method of Lines*, Master Thesis, Department of Mathematics, Chosun University, 2013.
[10] T. Johansson and B. D. Sleeamn, *Reconstruction of an acoustically sound-soft obstacle from one incident field and the far field pattern*, IMA J. Appl. Math. **72**(2007), 96-112.
[11] J. Kong, *Electromagnetic Wave Theory*, 2nd Ed., Wiley, New York, 1990.
[12] J. Lee and S. Kang, *Complex nonlinear parameter estimation(CNPE) and obstacle shape reconstruction*, Computers and Mathematics with Applications **67** (2014), 1631-1642.
[13] J. Lee and S. Kang, *Obstacle shape reconstruction by locally supported basis functions*, Honam Mathematical Journal **36** (2014), 831-852.
[14] K. Leem, J. Liu, and G. Pelekanos, *Two direct factorization methods for inverse scattering problems*, Inverse Problems **34** (2018), 125004 (26pp).
[15] J. Ma, T. Chia, T. Tan, and K. See, *Electromagnetic wave scattering from 2-D cylinder by using the Method of Lines*, Microwave and Optical Technology Letters **24(4)**(2000), 275-277.
[16] D. Nguyen, M. Klibanov, L. Nguyen,m A. Kolesov, M. Fiddy, and H. Liu, *Numerical solution of a coefficient inverse problem with multi-frequency experimental raw data by a globally convergent algorithm*, J. Computational Physics **345** (2017), 17-32.

Ju-Hyun Lee
Department of Mathematics, Chosun University,
Gwangju 501-759, South Korea
E-mail : juhyunlee@chosun.ac.kr

Nayoung Jeong
Department of Mathematics, Chosun University,
Gwangju 501-759, South Korea
E-mail : J-nayoung@nate.com

Sungkwon Kang
Department of Mathematics, Chosun University,
Gwangju 501-759, South Korea
E-mail : sgkang@chosun.ac.kr